Materials Research. 2024; 27:e20240332
DOI: https://doi.org/10.1590/1980-5373-MR-2024-0332

Investigation of Relationship Between Cooling Rate, Microstructure, Porosity and Corrosion in As-Cast Samples of the 1050 Aluminum Alloy Subjected to Different Levels of Gamma Radiation

***Wysllan Jefferson Lima Garção*[a], *Davi Ferreira de Oliveira*[a], *Olga Maria de Oliveira Araújo*[a],**

Cesar Giron Camerini*[b], *Elivelton Alves Ferreira*[c], *Alexandre Furtado Ferreira*[c]***

[a]*Universidade Federal do Rio de Janeiro, Laboratório de Instrumentação Nuclear, 21941-913, Rio de Janeiro, RJ, Brasil.*
[b]*Universidade Federal do Rio de Janeiro, Departamento de Engenharia Metalúrgica e de Materiais, Laboratório de Ensaios Não Destrutivos, Corrosão e Soldagem, 21941-913, Rio de Janeiro, RJ, Brasil.*
[c]*Universidade Federal Fluminense, Programa de Pós-Graduação em Engenharia Metalúrgica, 27255-125, Volta Redonda, RJ, Brasil.*

Received: July 31, 2024; Accepted: August 16, 2024

In this study, cellular spacing, porosity and corrosion of 1050 aluminum alloy subjected to the different levels of Gamma radiation was examined using a Gammacell Co-60 type irradiator, with activity of 16.13 TBq and dose rate around 6.98 Gy/min. Samples were extracted from an aluminum ingot, which was obtained with directional solidification apparatus. This upward directional solidification technique allowed obtaining of aluminum samples under different conditions of cooling rates. Firstly, cooling rates were determined during solidification experiment and then correlated to the cellular spacings and porosity content. The experimental results pointed out that cooling rates exerts a strong effect on the microstructural patterns and porosity formation. Laws have been determined, indicating that increase in cooling rates favored a refinement effect on as-cast microstructure and a decrease in porosity content. Furthermore, measurable effects of different levels of the Gamma radiation on the microstructure, porosity and corrosion for samples of 1050 aluminum alloy, were determined. The experimental results show that Gamma radiation has favored changes in cellular spacings, porosity formation and corrosion behavior. From this results, one can conclude that coarser microstructures, porosity formation and corrosion are favored by prolonged thermal annealing caused by temperature field generated during Gamma radiation exposure. On the other hand, even after the exposure to different levels of Gamma radiation, the microstructure and porosity observed in as-cast samples are still strongly dependent of the cooling conditions.

Keywords: *Gamma radiation, as-cast microstructure, porosity, corrosion, cooling rate.*

1. Introduction

Directional solidification with transient regime of heat extraction, allows study of the formation of solidified layers and microstructural evolution as a function of the cooling conditions. For upward solidification case, the melt ahead of the solid/liquid interface is enriched with solute segregated from the newly solidified layers[1-7]. The melt flows downward, and the convection phenomenon is limited between interdendritic/intercellular regions, since the thermal gradient tends to stabilize density stratification in the melt. These events lead to cell/dendrite fragmentation to accommodate high solute concentration in these regions[8].

Sales et al.[5] investigated the effects of solidification thermal parameters on the dendrite arm spacings and microhardness in directionally solidified binary Al-Si alloys. Experimental results obtained by authors, indicated an increase in arm spacings with the reduction in solidification speed and cooling rate. However, an increase in microhardness was observed with higher solidification speeds and cooling rates.

The convection effects on the dendritic patterns were considered by Spinelli et al.[7] in a downward directional solidification apparatus. Data for hypoeutectic Sn-Pb alloys pointed out that dendritic spacings can be strongly influenced by the solidification direction during the experiment.

Aluminum alloys have been adopted in a myriad of industrial applications, such as aerospace, automotive, shipbuilding and nuclear. This is mainly due to its intrinsic characteristics, i.e., good strength, reduced density, ease recycling and high corrosion resistance. The good characteristics observed in aluminum alloys have made it one of the most used nonferrous metals and stand a great potential to outperform other materials, such as steels and copper alloys, in most industrial applications. The ability of aluminum alloys to capture neutron is low, which favors good corrosion resistance, particularly in aquatic systems.

*e-mail: alexandrefurtado@id.uff.br

This property has designed aluminum alloys as a good choice for components of nuclear reactors, e.g., it is adopted as a tank material for TRIGA Mark Reactors, according to the Yıldırım et al.[9].

On the other hand, the penetrating power of Gamma rays, has many industrial applications. Gamma rays penetrate in several materials, however, this does not make them radioactive. Some uses of Gamma rays include medical equipment sterilization, thickness gauges in food packaging, and steel mills. Despite research proposed on the effects of Gamma radiation on the corrosion behavior in aluminum alloys, there has been conflict in agreeing on how radiation affects corrosion in aluminum alloys. Some authors have concluded that radiation does not affect the corrosion behavior in aluminum alloys of an aquatic environment, while other authors have a dissenting opinion, suggesting that radiation can accelerate the corrosion process of aluminum alloys[9-13]. Krenz[10] studied the corrosion of aluminum alloys with elements such as Ni, Fe and Si for several hours in a water-cooled reactor under high temperature and concluded that radiation can favor corrosion in these materials. Stobbs and Swallow[11] reached similar conclusions. The results obtained by Authors present indications that radiation favors the corrosion process in aluminum. Kanjana et al.[12], in turn, stated that Gamma radiation favors aluminum oxide development on the material surface due to the increased density of oxide with extended radiation and dose time. The formation and accumulation of radiation-induced defects and the role of lamellar interfaces in radiation damage of aluminum alloys was studied by Zhu et al.[14]. The results found by Zhu et al.[14] pointed out that dot-like defects first formed in the α_2-Ti_3Al and γ-TiAl phases of the irradiated microstructure. With increasing radiation dose, planar defects formed and propagated within the γ phase, and most of the planar defects were accompanied by the dot-like defects. According to the authors, the origins of the dot-like and planar defects are due to the interstitial clusters and stacking faults, respectively. The interstitial clusters formed and grew in the irradiated microstructure due to much faster diffusion of interstitials that of vacancies at room temperature. Local stress concentrations increased near large interstitial clusters and lamellar interfaces, resulting in the nucleation and propagation of stacking faults.

The radiation causes significant changes in the microstructure and mechanical properties of component materials in the reactors. Lattice displacement due to atomic collisions with high energy neutrons can introduce different types of defects in crystalline structure including; dislocation loops, cavities and other tiny defects. Hence, the microstructure changes may alter the mechanical properties through hardening and reduce ductility and fracture toughness. In addition, radiation damage of fast neutrons may affect the stability of the strengthening precipitates[9,10].

The main novelty of the present work is based on the fact that the effects of different levels of Gamma radiation on the as-cast samples of 1050 aluminum, were systematically investigated. We highlighted the measurable effects of Gamma radiation exposure on the microstructure, porosity content and corrosion. The ingot of 1050 aluminum alloy was obtained using an upward vertical solidification apparatus and the solidification experiment was carried out under transient conditions of heat extraction. A water-cooled system was used to investigate the effects of cooling rate on the cellular spacings and porosity content in as-cast samples of the 1050 aluminum alloy. Among the experimental results, the different doses influence of Gamma radiation (Co–60 source) on the changes in cellular spacings, porosity and corrosion stands out. It is important to highlight that even after the Gamma radiation exposure, microstructure and porosity, are still dependent on the solidification thermal conditions.

2. Experimental Procedure

The chemical composition of 1050 aluminum alloy is shown in Table 1.

An ingot of 1050 aluminum alloy was melted in a muffle furnace at 800°C. During the melting, a steel rod with a 1 mm thick layer of insulating alumina was used to ensure homogeneity of the melt. Subsequent to melting in muffle furnace, the 1050 aluminum alloy was cast into an upward unidirectional solidification apparatus with a water-cooled system, which allows high cooling rates at regions close to the mold bottom. Figure 1 shows the details of the solidification apparatus used in the present work. Details on the apparatus can be found in the literature[2,5,15].

The inner vertical surface of solidification furnace was covered with a layer of insulating alumina to reduce the radial heat flux. A cover made of refractory material was used on the mold top to minimize heat losses from the metal/air interface. The steel mold has internal diameter of 50 mm and a height of 140 mm. Its bottom was closed with a steel chill with a thickness of 3 mm, without layer of insulating alumina. The solidification apparatus has lateral electric heaters, so the desired superheat can be achieved before the start of the experiment per se. To begin solidification, the electric heaters are shut off while, at the same time, the water-cooling system is turned on. The experiment was carried out for 1050 aluminum alloy with a superheat of 10% above the melting temperature (T_m = 658 °C). Temperature profiles were determined by monitoring through a bank of type k thermocouples positioned along the casting at 5, 10, 15, 20, 35, 45, 60 and 85 mm from mold bottom. Temperature readings were collected by data acquisition system (data-logger hardware) at 0.001 second intervals to allow for an accurate determination of the thermal parameters. The readings were automatically stored on a personal computer. After the solidification experiment, the cylindrical ingot was sectioned along its vertical axis, mechanically polished with abrasive paper, and subsequently etched with an acid solution (25 ml H_2O, 2.5 ml HF, 25 ml HNO_3; 60 ml HCl) to

Table 1. Chemical composition of 1050 aluminum alloy.

Elements	Cu	Mg	Si	Fe	Mn	Zn	Ti	Al
weight (%)	0-0.05	0-0.05	0-0.25	0-0.4	0-0.05	0-0.07	0-0.05	bal.

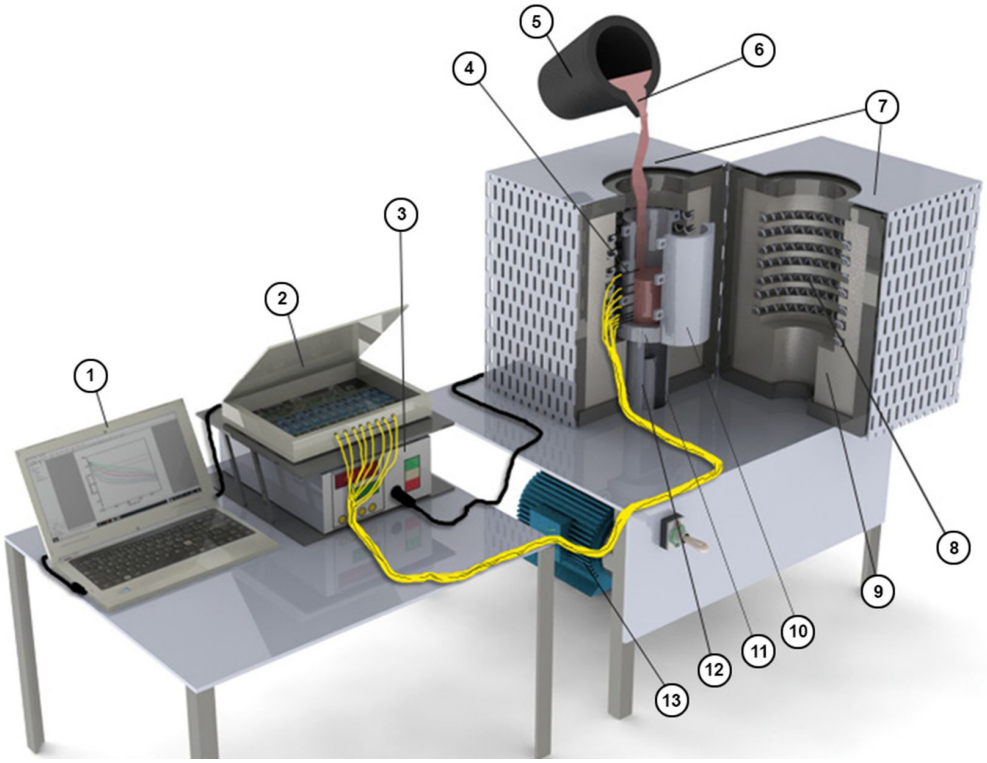

Figure 1. Diagrammatic representation of experimental apparatus: (1) personal computer and data acquisition software; (2) data-logger hardware; (3) temperature control system; (4) type k thermocouples; (5) crucible; (6) melt; (7) unidirectional solidification furnace; (8) electric heaters; (9) ceramic fiber insulation; (10) steel mold; (11) steel plate; (12) water-cooling system; and (13) water pump.

reveal its macrostructure. After the macrostructural analysis, selected transverse sections of the directionally solidified samples at 5, 10, 15, 20, 35, 45, 60 and 85 mm from the mold bottom were polished and etched with a solution 0.5% HF for micrograph examination. It is worth mentioning that the thermocouples maintained their positions even after the experiment, as shown in Figure 2.

Through temperature data collected during experiment, it was possible to determine the cooling rates ($\dot{\mathbf{T}}$) values for eight positions along the casting. The cooling rates ($\dot{\mathbf{T}}$) were determined considering the temperature (**T**) versus time (**t**) data immediately after the passage of the melting temperature ($\mathbf{T_m}$) for the different positions, as described by Ferreira et al.[6].

An Olympus Optical Microscope (Olympus Corporation, Japan) was used to produce digital images that were analyzed using the Goitaca (https://sourceforge.net/projects/goitacaeq) image processing software to measure cellular spacings (λ_C). Figure 3 is a representative micrograph of a transverse section from which cellular spacing (λ_C) measurements were made. About 20 measurements were taken for each position, with local cellular spacing (λ_c) being equal to average value. The method adopted for measuring the λ_C was the triangle method, according to the Silva et al.[16].

To characterize the pores observed both after solidification experiment and Gamma radiation exposure, eight samples were cut from the transverse directional planes, from the mold bottom to its top. These samples were assembled in conducting

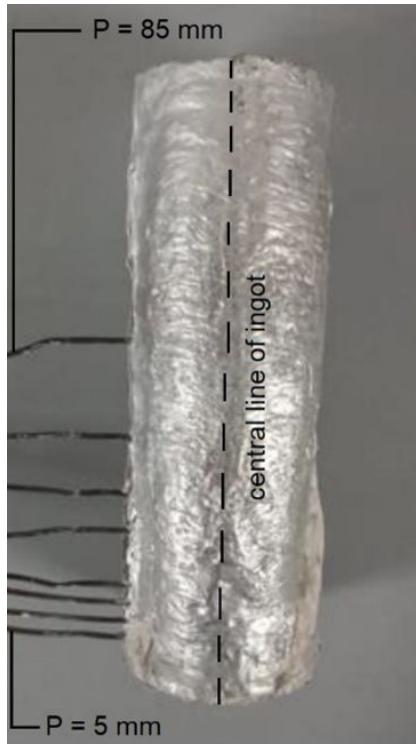

Figure 2. 1050 aluminum ingot with thermocouples positioned close to the central line.

Bakelite and polished to a 0.05 μm finish. The samples were analyzed using a Phoenix Vtomex m GE microtomograph equipped with two X-ray tubes and Flat-Panel DXR type detector. The acquisition parameters included a voltage of 100 kV, current of 150 μA, and a voxel size of 15 μm. This process involved generating 1500 projections with a total acquisition time of 15 minutes. Porosity analysis of the images was conducted using the CT Analyzer software (v. 1.16.4.1). A region of interest (ROI) measuring 8 mm x 10 mm x 3 mm was selected across 200 slices. A grayscale slice can be seen in Figure 4 below.

To study the radiation effects on the as-cast samples of 1050 aluminum alloy, the samples were irradiated using a Co-60 Gammacell (Nordion) at the Nuclear Instrumentation Laboratory of the Federal University of Rio de Janeiro (**UFRJ**), with activity of 16.13 TBq and dose rate around 6.98 Gy/min. Doses of Gamma radiation used in this experiment were 10, 25, 50, 100, 150 and 200 kGy. These doses were chosen to suit the routine use in radiosterilization process in products and foods.

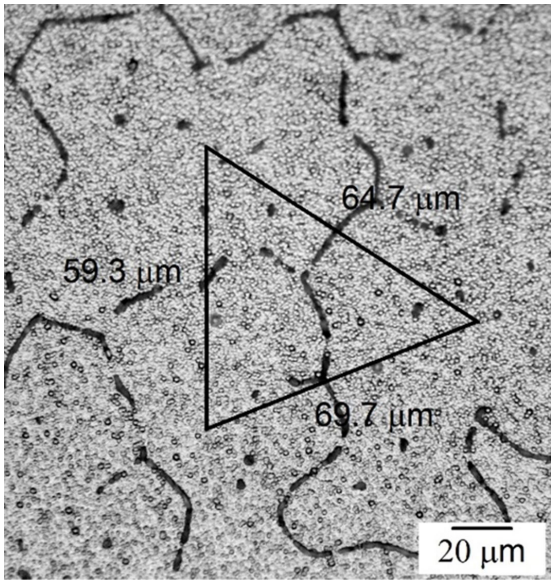

Figure 3. Schematic illustration of the cellular spacing (λ_c) measurements of 1050 aluminum sample.

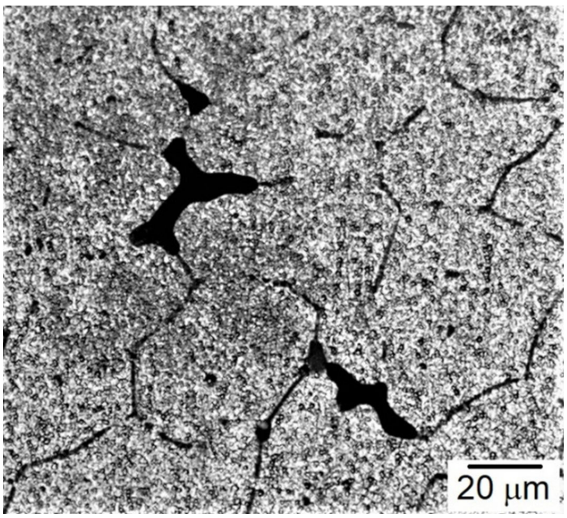

Figure 4. Image obtained from a Phoenix Vtomex m GE microtomograph of the irregular shape porosity for sample of 1050 aluminum.

The as-cast microstructure of aluminum alloys can be characterized by presence of the intermetallic particles, which exhibit different electrochemical activity compared to the matrix, leading to the onset of corrosion phenomena associated with local galvanic cells. In the last decade, electrochemical impedance spectroscopy (**EIS**) has been used as a tool to study features associated with corrosion process. This technique is based on the calculation and analysis of different local impedances acquired by a bi-electrode probe positioned in the vicinity of the electrode surface.

One of the aims of the present work was to study corrosion of the as-cast samples obtained from 1050 aluminum alloy, in sulfate containing media using electrochemical impedance spectroscopy (**EIS**). **EIS** Measurements were carried out through eight electrode cells at 24 °C. Samples of 1050 aluminum alloy were mounted in epoxy resin, and one face was left exposed to carry out the **EIS** tests. Its electric contact was sealed with a thin copper wire. Cells were positioned inside a Faraday cage in order to avoid electromagnetic disturbances. The impedance diagrams were determined in the frequency range from 40 kHz to 1 MHz, with disturbance amplitude of 20 mV peak using a Gamry potentiostat (Model Reference 600+), after 3600 sec stabilization of open circuit potential, controlled by a personal computer. A three-electrode configuration was used, a platinum electrode as counter electrode, saturated calomel electrode as the reference and aluminum sample as working electrode. A solution with 3.5% NaCl was used to perform the **EIS** test. The **SEM** analysis was carried out in a Jeol JSM 6301F microscope.

3. Results and Discussion

This work is divided into three parts. The first part is focused on cooling conditions effects on the cellular spacings (λ_C) and porosity formation during solidification experiment. Second part deals of effects of Gamma radiation exposure on the cellular spacings, porosity and corrosion for samples of the 1050 aluminum alloy. Finally, in the third part, cooling rates effects on the as-cast microstructure and porosity content after Gamma radiation exposure are presented and discussed.

3.1. Relationship between cooling rate, cellular spacing and porosity for 1050 Aluminum alloy before gamma radiation exposure

A file containing the temperature versus time data for the directional solidification experiment with transient conditions of heat extraction is presented in Figure 5. This graph shows the cooling curves obtained by means of the eight thermocouples placed at positions from the 5 to 85 mm along the casting height. The pouring temperature was set at around 750 °C, according to the Ferreira et al.[6]. It is observed that temperature curves decrease faster at regions close to the water-cooled bottom. The temperature curves slope then gradually dwindles with

solidification time. One can see to the right side of graph, information concerning the number of the sample, as well as position (**P**) along the as-cast material. These curves in Figure 5, presented profiles similar to those found in the open literature, Sales et al.[5]. From the Figure 5, cooling rate ($\dot{\mathbf{T}} = \mathbf{DT/dt}$) is correlated with position (**P**) of each thermocouple. It should be mentioned that the cooling rates ($\dot{\mathbf{T}}$) were determined from the temperature and time values recorded after the passing of the liquidus front ($\mathbf{T_m}$) by each position.

Figure 6 shows results concerning cooling rates ($\dot{\mathbf{T}}$) and cellular spacing (λ_c) as a function of position (**P**). One can see that the cooling rate ($\dot{\mathbf{T}}$) values decrease very fast in the regions close to the mold bottom, followed by a gradual decrease over the casting length. These behaviors are known and discussed in the literature[15,17,18]. Using water-cooling system during solidification favors high cooling rates close to the mold bottom. Farther away from bottom, the thermal parameter tends to decrease along the casting. This happens due to increase thermal resistance of the new solidified layers.

In the present work, the cooling rate determined during experiment was favored by water-cooled system and high thermal conductivity of 1050 aluminum alloy. According to the Tzou et al.[19], thermal conductivity of aluminum is about 220 W/m K. The cooling rate ($\dot{\mathbf{T}}$) presented in Figure 6, which is correlated to position of the as-cast material, is an aspect acting during the solidification, which affect the changes in the size and morphology of the as-cast microstructures. These microstructures, in turn, exerts an effect on the mechanical properties in the casting, Paradela et al.[15]. This dependence of cellular spacing (λ_C) with cooling rate ($\dot{\mathbf{T}}$), is depicted in Figure 7.

The dependence translates to the change in λ_c, i.e., high values of $\dot{\mathbf{T}}$, which are found in regions close to the mold bottom, favors a more refined microstructure and lower values of this thermal parameter close to the mold top, contribute effectively to a coarser microstructure. From the analysis of these results, it can be concluded that the increase in the thermal parameter reduce the possibility of cellular growth during solidification.

Since it is well known that aluminum alloys are susceptible to porosity formation during solidification, in order to avoiding or inhibit this type of defect, the present work was elaborated in this framework, emphasizing effects of the cooling rate ($\dot{\mathbf{T}}$) on the porosity found along casting. Figure 8 depicts the porosity content ($\mathbf{P_C}$) measured along the casting, taken from the bottom to the top of the aluminum ingot. The results for cooling rate ($\dot{\mathbf{T}}$) are plotted in this same graph, for comparison purposes. One can see that porosity content ($\mathbf{P_C}$) increases clearly with increasing position (**P**). This dependence on position (**P**) is related to the fact that the upward unidirectional solidification technique allows wider range of cooling rates ($\dot{\mathbf{T}}$) during experiment. This solidification apparatus with water cooled system is very useful when high rates of heat extraction to be achieved. A curve fitting technique from the experimental data has generated power function ($P_C = 0.0022P^{1.263}$), in order to represent the effect of position in the casting, on the porosity content.

The relationship between cooling rate ($\dot{\mathbf{T}}$) and porosity content ($\mathbf{P_C}$) is represented in Figure 9.

The porosity content ($\mathbf{P_C}$) decreases significantly with increasing cooling rate ($\dot{\mathbf{T}}$). Two effects that contribute to

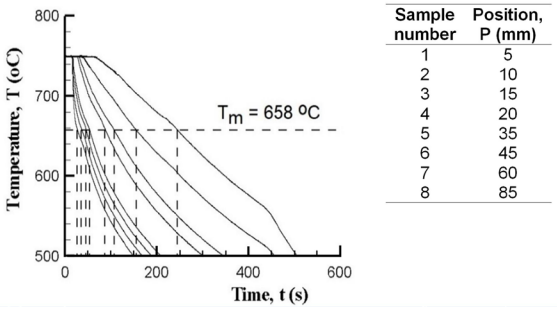

Sample number	Position, P (mm)
1	5
2	10
3	15
4	20
5	35
6	45
7	60
8	85

Figure 5. Temperature (**T**) versus time (**t**).

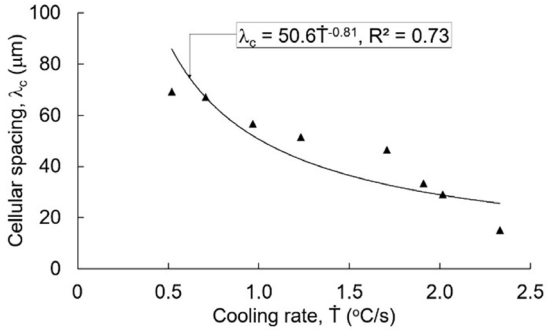

Figure 7. Cellular spacing (λ_c) versus cooling rate ($\dot{\mathbf{T}}$).

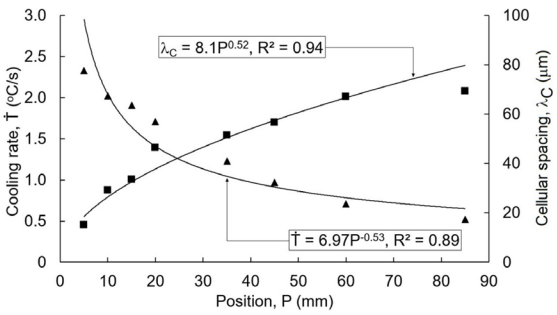

Figure 6. Cooling rate ($\dot{\mathbf{T}}$) and cellular spacing (λ_c) versus position (**P**).

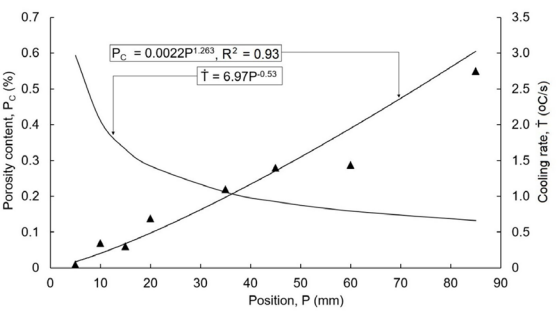

Figure 8. Porosity content ($\mathbf{P_C}$) and cooling rate ($\dot{\mathbf{T}}$) versus position (**P**).

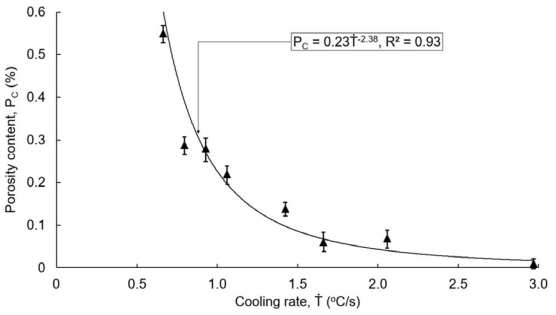

Figure 9. Porosity content ($\mathbf{P_C}$) versus cooling rate ($\dot{\mathbf{T}}$).

the formation of porosity during solidifying aluminum, are the shrinkage resulting from the volume decrease in going from liquid to solid phase, and gas evolution resulting from the decrease in solubility in solid compared to the liquid region. Both phenomena observed in present work, can occur simultaneously and act synergistically to develop porosity during solidification. When the aluminum solidifies, solubility of hydrogen in the liquid is decreased and gas porosities can be formed. When water-cooled mold system is applied, high cooling rates ($\dot{\mathbf{T}}$) are obtained close to the bottom and gas in this region is supersatured. This avoids nucleation of gas porosity, so content of gas porosity can be minimized. The water-cooled system, as previously discussed, are usually used to optimize the cooling rates ($\dot{\mathbf{T}}$), and have several advantages as finer grain structure, decrease of microstructural spacing and decrease of shrinkage cavities. So, it is to be expected that high cooling rates ($\dot{\mathbf{T}}$) close to the mold bottom, also favors decrease in shrinkage porosity. Since the cooling rates ($\dot{\mathbf{T}}$) depend on the position in casting, the values of porosity content ($\mathbf{P_C}$) vary in the distribution of these cooling rates proportionally, Figure 9. Typical cellular microstructure with shrinkage and gas porosity, can be observed along the transverse sections of the aluminum alloy directionally solidified, Figure 10. These porosities manifest themselves in different ways in casting. They form in the mushy zone, and their morphologies and extent are very distinct. Morphology of gas porosity, Figure 10a, resembles a spherical shape, while shrinkage porosity morphology is almost always irregular and elongated, Figure 10b. By considering the micrographs presented in Figure 10, we can conclude that the two main causes of porosity were found during solidification of 1050 aluminum alloy: a) Gas porosity, due to the dissolved gases in the melt upon freezing; and b) Shrinkage porosity, due to the volume change upon solidification. Cellular microstructure can be observed along the transverse sections of the 1050 aluminum alloy directionally solidified, Figure 10. Despite the relative high cooling rate imposed by the water-cooled system during the unidirectional solidification experiment, cellular microstructures were predominant in the casting. To the right side of Figure 10, information can be found concerning the position (**P**), cellular spacing (λ_C), cooling rate ($\dot{\mathbf{T}}$) and type of porosity observed in as-cast sample.

Table 2 that follow, presents position (**P**) in which the samples were taken in the casting, cooling rates ($\dot{\mathbf{T}}$), cellular spacings (λ_C) and porosity content ($\mathbf{P_C}$).

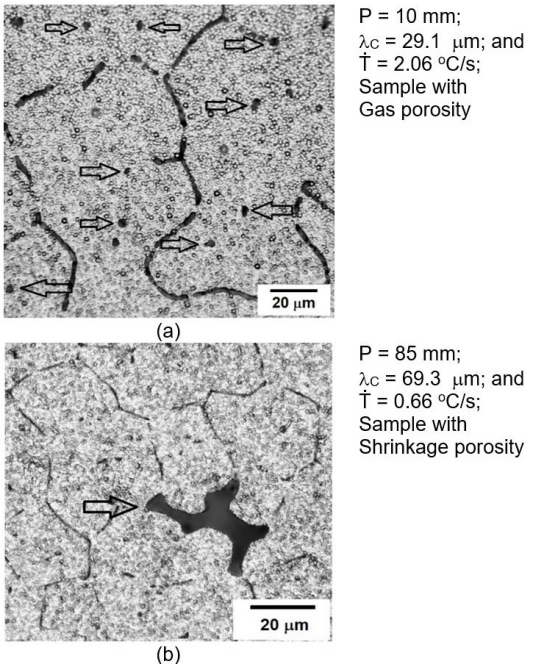

Figure 10. Porosity as observed at different distance from water-cooled bottom: a) P = 10 mm; and b) 85 mm.

One can see in Table 2, that thermal condition of solidification (cooling rate) servers to condition the changes not only microstructural spacings itself but also the porosity formation along the as-cast aluminum alloy, affecting strongly the quality of the final product.

3.2. Effect of Gamma radiation exposure on the cellular spacing, porosity content and corrosion

Two samples of as-cast 1050 aluminum taken at positions of 5 and 45 mm were exposed to doses from 10 to 200 kGy and its effect on the cellular spacing (λ_C) are presented in Figure 11.

One can see that the cellular spacing profiles of the analyzed cases are clearly nonlinear. Both curves show an increasing profile with increase in Gamma radiation level. It is worth mentioning that cellular spacing (λ_C) determined before Gamma radiation exposure, for samples n. 1 and n. 6 taken at position of 5 and 45 mm, was 15.2 and 56.7 μm, respectively, as indicated in Table 2. For lowest Gamma radiation level (Gr = 10 kGy), both samples, n. 1 and n. 6, already showed an increase in cellular spacings of 20.0 and 58.2 μm. These experimental data point out that 1050 aluminum alloy when submitted to Gamma radiation, from 10 to 200 kGy, which required a high exposure time and high temperatures, lead to a coarser microstructure. The factor influencing the coarser microstructures during Gamma radiation exposure is due to prolonged thermal annealing caused by temperature field generated during radiation test, as reported by Munitz et al.[20].

As previously discussed, a severe type of defect that can be observed during solidification is porosity, and aluminum

alloys are susceptibility to formation of this defect, as reported by Dantas et al.[21]. In the present paper, the porosity behavior was studied before and after Gamma radiation exposure, as shown in Figure 12.

The non-radiated samples n. 5 and n. 8, i.e., obtained through solidification experiment before Gamma radiation exposure, presented a porosity content of 0.22 and 0.54%, as shown in Table 2. The porosity dependence on the radiation dose can be observed in those graphs, where the increase in porosity content is observed with doses of Gamma radiation from 25 kGy for sample n. 5 and 50 kGy for as-cast sample n. 8. Through the analysis of these data, it can be concluded that after Gamma radiation exposure of 200 kGy, the sample n. 5 had its porosity content increased by about 40%, while the

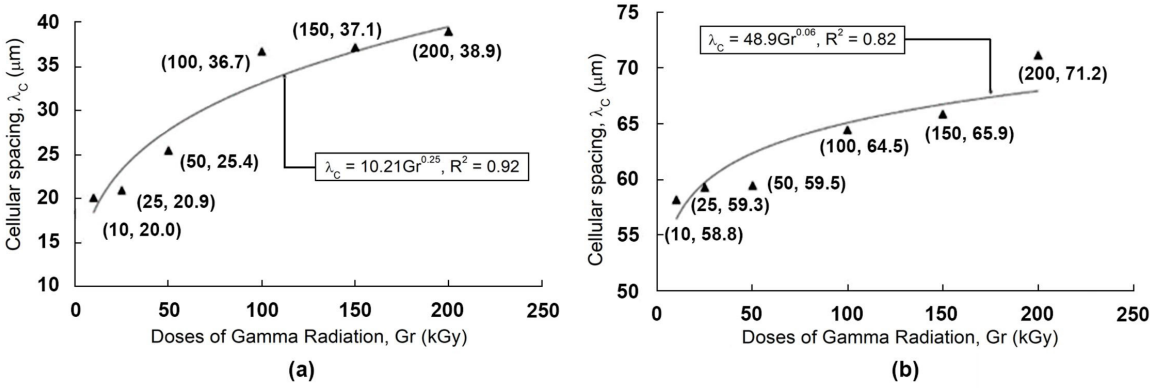

Figure 11. Cellular spacing (λ_C) versus Gamma radiation (**Gr**): a) Sample n. 1 taken at P = 5 mm; and b) Sample n. 6 taken at P = 45 mm.

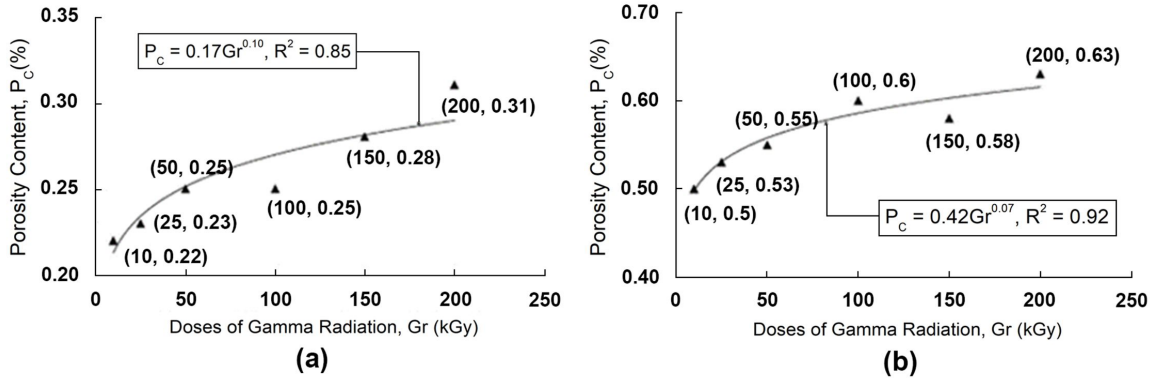

Figure 12. Porosity content ($\mathbf{P_C}$) versus Gamma radiation (**Gr**): a) Sample n. 5 taken at P = 35 mm; and b) Sample n. 8 taken at P = 85 mm.

Table 2. Cooling rate, cellular spacing and porosity content along the as-cast aluminum alloy 1050.

Sample number	Position, P (mm)	Cooling rate, $\dot{T}$ (°C/s)	Cellular spacing, λ_C (μm)	Porosity content, P_C (%)
1	5	2.97	15.2	0.01
2	10	2.06	29.1	0.07
3	15	1.66	33.4	0.06
4	20	1.42	46.4	0.14
5	35	1.05	51.4	0.22
6	45	0.92	56.7	0.28
7	60	0.79	67.0	0.29
8	85	0.66	69.3	0.54

sample n. 8 shows an increase of 63%. For both cases, it can be seen that porosity content ($\mathbf{P_C}$) values increase with doses of Gamma radiation (**Gr**). According to Kanjana et al.[12], the increase in porosity is due to the fact that Gamma radiation dose accelerates the corrosion process in aluminum alloys. Although aluminum alloys are known to develop highly stable aluminum oxides, corrosion process in this group of materials has commonly been observed in water-cooled Research Reactor. According to the Munitz et al.[20] and Yahr[22], corrosion process in these alloys is believed to be mostly attributed to ionizing radiations. According to the Authors, ionizing radiation can interact with material and its effects can result in lattice vacancies, self-interstitial atoms and transmutation products (radiation damage microstructures). As of now, the ionizing radiation effects on corrosion of materials are still not yet fully understood. Only limited information regarding radiation-induced/accelerated corrosion of aluminum alloys is available in literature.

Due to the aforementioned fact, the present work also was focused on the effects of Gamma radiation exposure on the corrosion behavior of the 1050 aluminum alloy. The results are presented and discussed below. A plot for the open circuit potential (**E**) versus time (**t**) is reported in Figure 13. One can see in that figure, a discrepancy between the open circuit potential (**OCP**) profiles for as-cast samples.

The more negative values displayed in the as-cast aluminum sample n.8 (-1.02 V), as compared to the sample n. 1 (-0.92 V), can be related to the as-cast microstructure formation during the solidification experiment. According to the Dantas et al.[21], more refined microstructures are observed in regions close to the mold bottom, while a coarser microstructure is found in regions near to the top. It is worth mentioning that water-cooled system favors high cooling rates in regions close to the mold bottom, and cooling rates, in turn, serve to condition the changes on microstructural spacings. The sample n. 1 was taken at position of 5 mm, while sample n. 8 was taken at 85 mm away from the water-cooled bottom. From data shown in Table 2, one can see that higher values of cooling rate were found in regions close to the mold bottom.

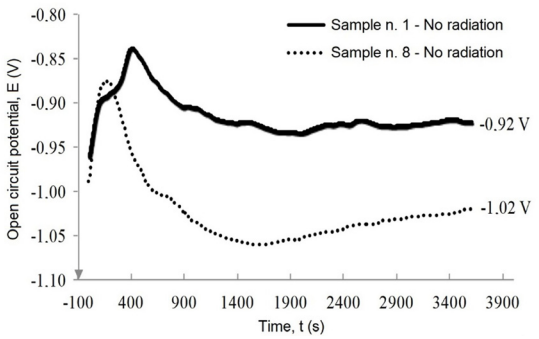

Figure 13. Open circuit potential versus time for as-cast samples before Gamma radiation exposure.

The values for open circuit potential for as-cast samples before and after Gamma radiation exposure for comparison purposes, are listed in Table 3. From the analysis of the Table 3, it can be concluded that values of OCP are more negative for as-cast aluminum samples exposed to the Gamma radiation (200 kGy) when compared to the as-cast aluminum sample before Gamma radiation exposure. Therefore, one can observe that after as-cast samples were exposed to Gamma radiation, they presented a less noble behavior, and as-cast samples with refined microstructures are more sensitive to the Gamma radiation exposure.

Figures 14 and 15 show corresponding experimental electrochemical impedance spectroscopy (**EIS**) diagrams, for as-cast aluminum samples before and after Gamma radiation exposure. In Impedance versus Frequency plot, Figure 14a, it can be observed that all samples present three distinct regions: a) from a frequency range below 20 mHz, the Bode diagrams exhibit an impedance response that can be ascribed to oxygen diffusive process, Liu et al.[23], b) around at 20 mHz, the Bode magnitude plots exhibits a |Z| value of around 10.0 kΩ.cm^2, which can represent oxide film resistance on the as-cast aluminum samples, c) in the higher frequency region, from 1.0 kHz to 0.10 MHz, exhibits |Z| values of up to 20 Ω.cm^2, which indicates that impedance is controlled by the electrolyte resistance, and d) in the broad low and middle frequency range, the Bode plot displayed a linear slope, which is a characteristic response of a capacitive behavior of the aluminum oxide film, Liu et al.[23]. Phase angle versus Frequency is shown in Figure 14b.

For different as-cast samples, before and after radiation application, it is possible to observe a phase constant answer at approximately 10 Hz that was associated with an oxide film on the samples, Liu et al.[23]. The samples n.1 and n.8 before and after Gamma radiation exposure presented the maximum phase angles 70.1, 65.5, 69.4, and 74.0°, respectively.

Figure 15 shows **EIS** results with Nyquist diagram. When analyzing the Nyquist diagram, different capacitive-resistive semicircles attributed to oxide film on samples can be found in the high-frequency range. At low frequencies, a diffusive tail was also observed in this diagram. In Figure 15a, one can see that the diameters of the capacitive-resistive semicircle increase with decreasing of cellular spacing (λ_C), i.e., from a fine microstructure array at the mold bottom to a coarse cellular array at the top. A higher diameter of the capacitive-resistive semicircle can be observed for the refined cellular microstructure, sample n.1, when compared with that of the

Table 3. Open circuit potential (**E**) for as-cast samples before and after Gamma radiation exposure.

	As-cast sample n. 1		As-cast sample n. 8	
	Before Gamma radiation exposure	After Gamma radiation exposure (200 kGy)	Before Gamma radiation exposure	After Gamma radiation exposure (200 kGy)
Open circuit potential, E (V)	-0.92	-1.02	-1.02	-1.07
Cellular spacing, λc (μm)	15.2	38.9	69.3	82.6

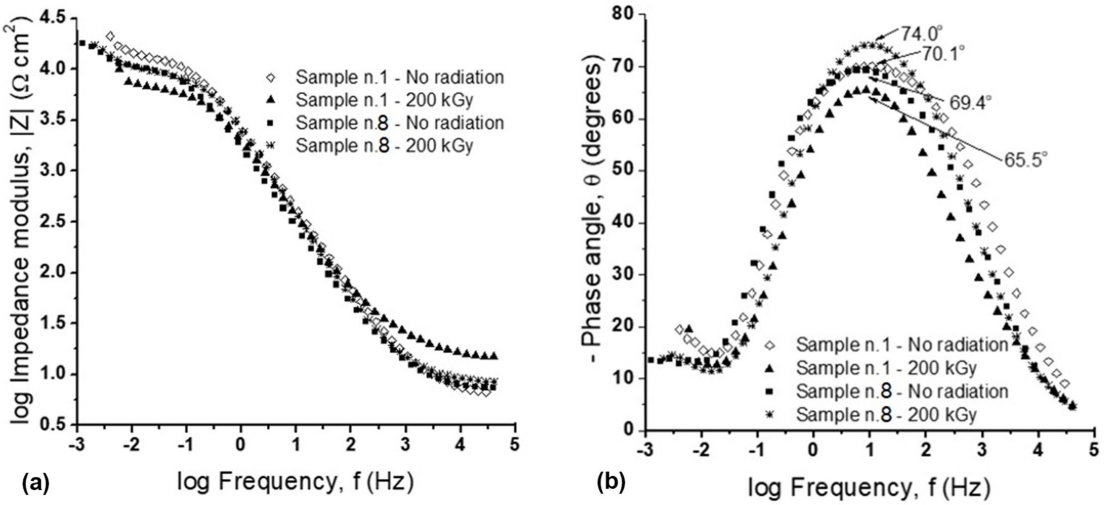

Figure 14. Experimental Bode diagrams for as-cast aluminum samples: a) Impedance module versus frequency; and b) Phase angle versus frequency.

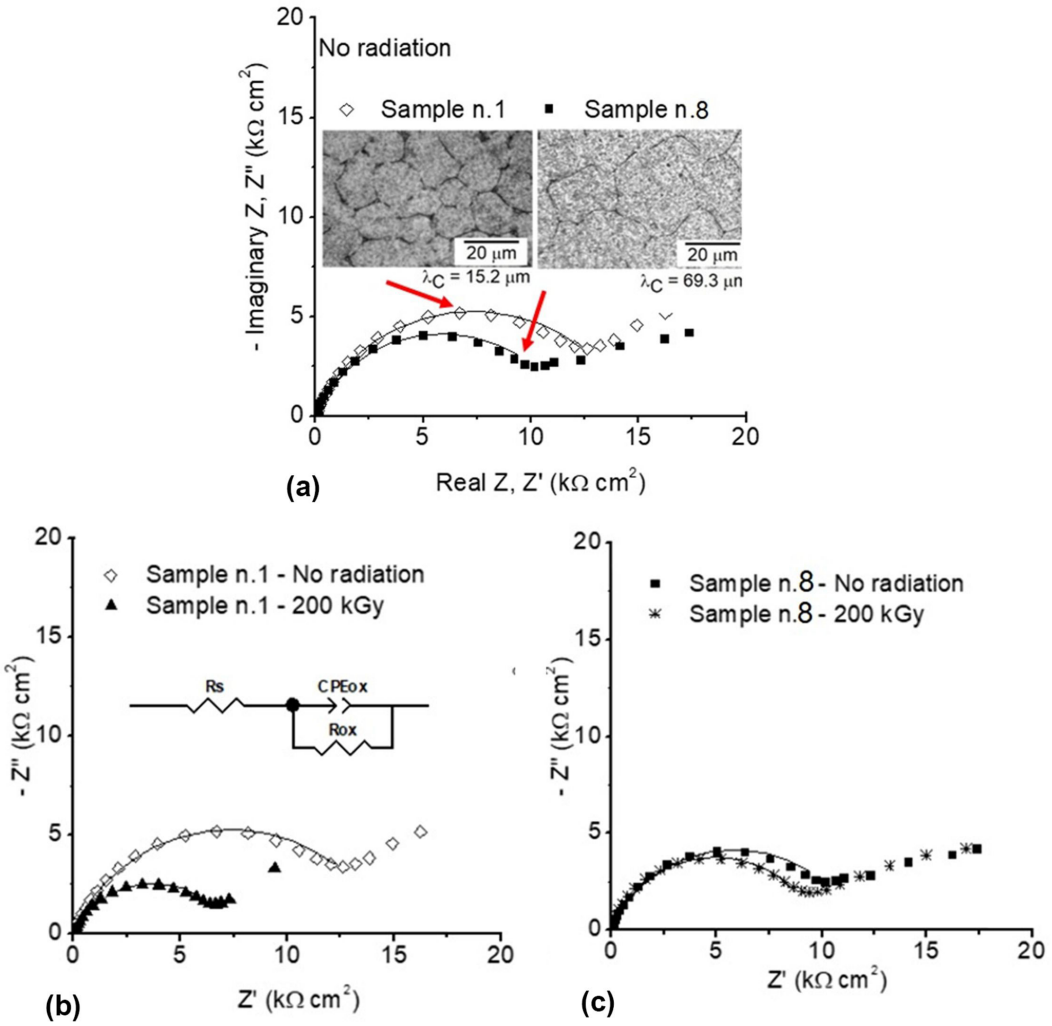

Figure 15. EIS results with Nyquist diagram adopted; a) Before Gamma radiation exposure for as-cast samples n. 1 and n. 8; b) Before and after Gamma radiation exposure for as-cast sample n.1; and c) Before and after Gamma radiation exposure for as-cast sample n. 8.

coarse microstructure, sample n. 8, (Figure 15a). Similar observations can also be made when considering the as-cast aluminum samples before and after radiation exposure, i.e., samples before Gamma radiation exposure presented a higher diameter of the capacitive-resistive semicircle when compared to the samples submitted to the Gamma radiation exposure, (Figure 15b and 15c). The Randles circuit (Figure 15b) was fitted using the Z-View® software to the impedance results of all samples in the high-frequency range assigned the first phase constant (continuous line in Nyquist representation in Figure 15a-c).

In this circuit, the R_s, CPEox-T, and Rox represent the solution resistance, the constant phase element of the oxide film, and the oxide resistance, respectively. For non-ideal capacitive responses, the CPE was considered in the fit of the equivalent electric equivalent. The CPE is expressed by CPE-T and CPE-P values (Table 4). If CPE-P equals 1, CPE-T is an ideal capacitor, but for CPE-P values between 0.9 and 1, the capacitor is considered non-ideal[24]. The oxide film resistance (R_{ox}) can be correlated with the corrosion resistance of the sample, Liu et al.[23]. Therefore, the corrosion resistance of the sample n. 1 and n. 8, before Gamma radiation exposure, were 14.7 Ω cm^2 and 11.7 Ω cm^2, respectively (Table 4). This decrease in corrosion resistance can be associated with the fine microstructure array change at the mold bottom (sample n.1) to a coarse cellular array at the top (sample n. 8). The coarser cellular array cannot be passivated more readily than the refined microstructure owing to lower grain boundary density, Ralston and Birbilis[24]. After Gamma radiation exposure, the samples n. 1 and n. 8 decrease the corrosion resistance from 14.7 Ω cm^2 and 7.5 Ω cm^2 to 11.7 Ω cm^2 and 9.7 Ω cm^2, respectively (Table 4). This changing behavior can be correlated with the neutron irradiation effect on a metallic material that can change its crystal structures, mechanical properties, and physical dimensions, Kanjana and Channuie[25]. Similarly, as happened with the corrosion resistance of the different samples, the microstructure difference between samples n. 1 and n. 8, and Gamma radiation exposure provided also changes in CPE values (Table 4). Finally, it is possible to observe that the as-cast aluminum with coarser microstructure (sample n. 8) presented less corrosion decrease after Gamma radiation exposure.

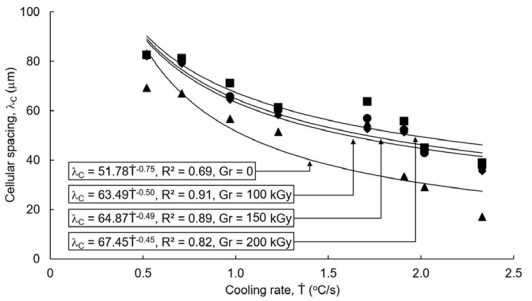

Figure 16. Cellular spacing (λ_C) versus cooling rate ($\dot{\mathbf{T}}$), after Gamma radiation exposure.

3.3. Effect of the cooling rates on the cellular spacing and porosity content after Gamma radiation exposure

With purpose of understanding the effects of cooling conditions on samples of 1050 aluminum alloy exposed to the Gamma radiation, relationships between cooling rates ($\dot{\mathbf{T}}$), cellular spacing (λ_C) and porosity content ($\mathbf{P}_C$) are presented and discussed. The first part of this section, is focused relationships between cooling rate ($\dot{\mathbf{T}}$) and cellular spacing (λ_C). About 20 measurements were carried out on samples taken along the casting length. These samples were submitted to the Gamma radiation exposure of 100, 150 and 200 kGy, results are presented in Figure 16.

One can see that profiles of cellular spacings move upward with the increase in Gamma radiation levels, i.e., as-cast samples submitted to the Gamma radiation have presented coarser microstructures. This is due to prolonged thermal annealing provoked by temperature fields generated during tests with high levels of radiation. Also, can be seen that even after the samples have been submitted to the Gamma radiation exposure, the profiles are clearly nonlinear, with values of cellular spacings (λ_C) increase with increasing cooling rates ($\dot{\mathbf{T}}$) determined along the casting. As the results for cellular spacings (λ_C) suggest, even after Gamma radiation exposure with prolonged thermal annealing provoked by temperature fields during tests of Gamma radiation, the cooling conditions observed during the solidification experiment, still exerts an effect on the as-cast microstructures patterns, Figure 16.

The effects of cooling rate ($\dot{\mathbf{T}}$) on the porosity ($\mathbf{P}_C$) behavior in as-cast samples after Gamma radiation exposure, are shown in Figure 17.

For any cases analyzed, porosity content decrease with increasing cooling rate, i.e. higher cooling rates have inhibited porosity formation. It is worth mentioning that said behavior was also observed, even after the as-cast samples

Table 4. Circuit elements values of Randles acquired from the fitting of the experimental impedance data.

EIS parameters	As-cast sample n.1		As-cast sample n. 8	
	Before Gamma radiation exposure	After Gamma radiation exposure (200 kGy)	Before Gamma radiation exposure	After Gamma radiation exposure (200 kGy)
Solution resistance, R_s (Ω cm^2)	6.8	16.2	7.6	9.0
Oxide film resistance, R_{ox} (kΩ cm^2)	14.7	7.5	11.7	9.7
Constant phase element, CPE_{ox}-T (μF cm^{-2} s^{n-1})	86.7	118.7	133.1	79.9
Constant phase element, CPE_{ox}-P	0.79	0.75	0.78	0.83

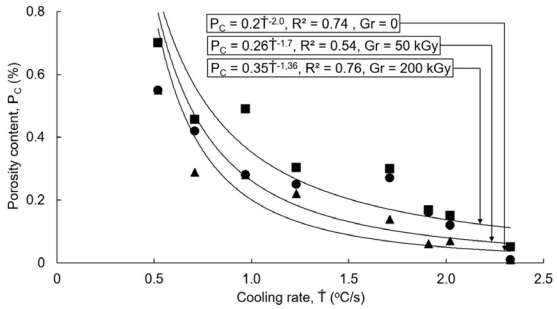

Figure 17. Porosity content ($\mathbf{P_C}$) versus cooling rate ($\dot{\mathbf{T}}$), after Gamma radiation exposure.

have been submitted to the Gamma radiation exposure. Through analysis of these results, it can be concluded that cooling conditions still exerts an effect on the porosity, even after the as-cast samples were submitted to the different levels of Gamma radiation. On the other hand, we can see in Figure 17 a discrepancy between the experimental profiles. The results pointed out that the Gamma radiation exposure (50 and 200 kGy) lead to an increase in porosity content. The increase in porosity for samples submitted to the Gamma radiation, is due to the fact that 1050 aluminum when radiation exposure, accelerates the corrosion process within pores.

4. Conclusions

This work examined the relationships between cooling rates, microstructural patterns, porosity and corrosion of the 1050 aluminum alloy subjected to the Gamma radiation. The conclusions are presented below.

1. For non-irradiated samples, the thermal conditions of solidification servers to condition the changes in cellular spacings and porosity, significantly impacting the final product quality;
2. Porosity formation decreases with cooling rates due to two main factors: a) when high cooling rates are applied in regions close to the mold bottom, gas in these regions is supersatured, so this avoids nucleation of gas porosity, and b) higher cooling rates favored a finer microstructure and a decrease in the shrinkage cavities, therefore it is to be expected that cooling rates favors a decrease in shrinkage porosity;
3. When subjected the samples of the 1050 aluminum alloy to the Gamma radiation, their cell microstructures became coarser. One can conclude that factor that favored coarser as-cast microstructures during Gamma radiation exposure is prolonged thermal annealing provoked by temperature field generated during radiation test;
4. Porosity was also increased after the samples were subjected to the Gamma radiation. Increase in porosity is due to the fact that samples of 1050 aluminum alloy when radiation exposure, accelerates the corrosion process inside the pores;
5. The electrochemical corrosion essays showed that the **OCP** was more negative for as-cast aluminum samples exposed to Gamma radiation (200 kGy) when compared to the sample before Gamma radiation exposure. It was possible to observe also that the as-cast sample with refined microstructure was less noble due to Gamma radiation exposure;
6. The **EIS** essays indicated that the as-cast samples exposed to the radiation were less corrosion-resistant. However, the corrosion resistance of the sample with a coarser microstructure was less affected by Gamma radiation; and
7. The results observed in this work, pointed out that even after the exposure to different levels of Gamma radiation, with higher exposure times and high temperatures, the microstructures and porosity are still strongly dependent of the cooling conditions during solidification.

5. Acknowledgments

The authors are grateful to National Council for Scientific and Technological Development (CNPq, nº 302847/2022-7, PQ - 2022) for financial support.

6. References

1. Baptista LAS, Ferreira AF, Paradela KG, Silva DM, Castro JA. Experimental investigation of ternary Al-Si-Cu alloy solidified with unsteady-state heat flow conditions. Mater Res. 2018;21(3):e20170565. http://doi.org/10.1590/1980-5373-mr-2017-0565.
2. Ferreira AF, Castro JA, Ferreira LO. Predicting secondary-dendrite arm spacing of the Al-4.5wt%Cu alloy during unidirectional solidification. Mater Res. 2016;20(1):68-75. http://doi.org/10.1590/1980-5373-mr-2015-0150.
3. Goulart PR, Cruz KS, Spinelli JE, Ferreira IL, Cheung N, Garcia A. Cellular growth during transient directional solidification of hypoeutectic Al–Fe alloys. J Alloys Compd. 2009;470(1-2):589-99. http://doi.org/10.1016/j.jallcom.2008.03.026.
4. Gündüz M, Çadırlı E. Directional solidification of aluminium–copper alloys. Mater Sci Eng A. 2002;327(2):167-85. http://doi.org/10.1016/S0921-5093(01)01649-5.
5. Sales RC, Ferreira LO, Almeida RP, Terra BP, Moura LJ, Ferreira AF. Microstructure and microhardness of directionally solidified Al-Si alloys subjected to an equal-channel angular pressing process. Mater Res. 2022;25:e20210344. http://doi.org/10.1590/1980-5373-mr-2021-0344.
6. Ferreira AF, Moura LJ, Dantas BS, Brum FJB, Garção WJL, Sales RC. Investigations on metallurgical parameters in hypoeutectic Al–Si alloys under upward directional solidifications. Int J Adv Manuf Technol. 2022;121(11-12):7359-82. http://doi.org/10.1007/s00170-022-09836-3.
7. Spinelli JE, Rocha OFL, Garcia A. The influence of melt convection on dendritic spacing of downward unsteady-state directionally solidified Sn-Pb alloys. Mater Res. 2006;9(1):51-7. http://doi.org/10.1590/S1516-14392006000100011.
8. Mathiesen RH, Arnberg L, Bleuet P, Somogyi A. Crystal fragmentation and columnar-to-equiaxed transitions in Al-Cu studied by synchrotron X-ray video microscopy. Metall Mater Trans, A Phys Metall Mater Sci. 2006;37(8):2515-24. http://doi.org/10.1007/BF02586224.
9. Yıldırım S, Tugrul AB, Buyuk B, Demir E. Gamma attenuation properties of some aluminum alloys. Acta Phys Pol A. 2016;4(129):813-5. http://doi.org/10.12693/APhysPolA.129.813.
10. Krenz FH. Corrosion of aluminum-nickel type alloys in high-temperature aqueous service. Corrosion. 1957;13(9):43-9. http://doi.org/10.5006/0010-9312-13.9.43.

11. Stobbs JJ, Swallow AJ. Effects of radiation on metallic corrosion. Int Mater Rev. 1962;7(1):95-132. http://doi.org/10.1179/095066062790207795.
12. Kanjana K, Ampornrat P, Channuie J. Gamma-radiation-induced corrosion of aluminum alloy: low dose effect. J Phys Conf Ser. 2017;860(1):12041. http://doi.org/10.1088/1742-6596/860/1/012041.
13. Kawaguchi M, Ishigure K, Fujita N, Oshima K. Effect of radiation on the release of corrosion products in a high-temperature aqueous system. Radiat Phys Chem (1977). 1981;18(3–4):733-40. http://doi.org/10.1016/0146-5724(81)90196-5.
14. Zhu H, Qin M, Aughterson R, Wei T, Lumpkin G, Ma Y, et al. The formation and accumulation of radiation-induced defects and the role of lamellar interfaces in radiation damage of titanium aluminum alloy irradiated with Kr-ions at room temperature. Acta Mater. 2020;195:654-67. http://doi.org/10.1016/j.actamat.2020.06.009.
15. Paradela KG, Baptista LAS, Sales RC, Felipe P Jr, Ferreira AF. Investigation of thermal parameters effects on the microstructure, microhardness and microsegregation of Cu-Sn alloy directionally solidified under transient heat flow conditions. Mater Res. 2019;22(4):e20190259. http://doi.org/10.1590/1980-5373-mr-2019-0259.
16. Silva BL, Garcia A, Spinelli JE. The effects of microstructure and intermetallic phases of directionally solidified Al–Fe alloys on microhardness. Mater Lett. 2012;89:291-5. http://doi.org/10.1016/j.matlet.2012.08.130.
17. Lingappa MS, Srinath MS, Amarendra HJ. Microstructural and mechanical investigation of aluminium alloy (Al 1050) melted by microwave hybrid heating. Mater Res Express. 2017;4(7):076504. http://doi.org/10.1088/2053-1591/aa7aaf.
18. Abdulstaar M, Mhaede M, Wagner L, Wollmann M. Corrosion behaviour of Al 1050 severely deformed by rotary swaging. Mater Des. 2014;57:325-9. http://doi.org/10.1016/j.matdes.2014.01.005.
19. Tzou GJ, Tsao CC, Lin YC. Improvement in the thermal conductivity of aluminum substrate for the desktop PC Central Processing Unit (CPU) by the Taguchi method. Exp Therm Fluid Sci. 2010;34(6):706-10. http://doi.org/10.1016/j.expthermflusci.2009.12.012.
20. Munitz A, Shtechman A, Cotler C, Talianker M, Dahan S. Mechanical properties and microstructure of neutron irradiated cold worked A1-6063 alloy. J Nucl Mater. 1998;252(1-2):79-88. http://doi.org/10.1016/S0022-3115(97)00293-6.
21. Dantas BS, Garção WJL, Peixoto FM, Guimarães NA, Tomaszewski IMS, Ferreira AF. Microstructural patterns, microsegregation, porosity, and mechanical properties of hypoeutectic Al-Fe alloy, and its dependency with solidification thermal parameters. Mater Res. 2022;25:e20220187. http://doi.org/10.1590/1980-5373-mr-2022-0187.
22. Yahr GT. Prevention of nonductile fracture in 6061-T6 aluminum nuclear pressure vessel. J Press Vessel Technol. 1997;119(2):150-6. http://doi.org/10.1115/1.2842276.
23. Liu Y, Meng GZ, Cheng YF. Electronic structure and pitting behavior of 3003 aluminum alloy passivated under various conditions. Electrochim Acta. 2009;54(17):4155-63. http://doi.org/10.1016/j.electacta.2009.02.058.
24. Ralston KD, Birbilis N. Effect of grain size on corrosion: a review. Corrosion. 2010;66(7):075005. http://doi.org/10.5006/1.3462912.
25. Kanjana K, Channuie J. Corrosion of neutron/gamma-irradiated aluminium alloy 6061. Songklanakarin J Sci Technol. 2019;41(2):445-9.